DONG THAP UNIVERSITY JOURNAL OF SCIENCE
Tạp chí Khoa học Đại học Đồng Tháp
Natural Sciences Issue
ISSN 0866-7675 | e-ISSN 2815-567X

DOI: https://doi.org/10.52714/dthu.ns.3329.2004

OPTIMIZING β-Ga_2O_3 NANOROD MORPHOLOGY BY CONTROLLING HYDROTHERMAL REACTION TIME FOR UVC PHOTODETECTION

Minh-Dat Duong[1], My-Duyen Mai-Dinh[1], Tien-Luat Nguyen[2], Quynh-Anh Hoang-Nguyen[1], and Huy-Binh Do[1]*

[1]Ho Chi Minh City University of Technology and Engineering, Vietnam

[2]Faculty of Materials Science and Technology, University of Science, Ho Chi Minh City, Viet Nam

**Corresponding author, Email: binhdh@hcmute.edu.vn*

Article history

Received: 10/4/2026; Received in revised form: 04/6/2026; Accepted: 11/6/2026

Abstract

β-Ga_2O_3 nanorods were synthesized by a hydrothermal method with growth durations of 5, 7.5, and 10 h to investigate the effect of growth time on their structural, morphological, and UVC photodetection properties. XRD analysis confirmed the formation of monoclinic β-Ga_2O_3 for all samples. Increasing the hydrothermal duration from 5 h to 7.5 h improved the crystal quality, as evidenced by an increase in crystallite size from 18.3 to 20.6 nm and the reduction in both microstrain and dislocation density. FE-SEM observations revealed well-developed nanorods at 7.5 h, whereas prolonged growth to 10 h resulted in aggregation and secondary growth. The optical sensor fabricated with the 7.5 h sample exhibited the highest photocurrent (~49 nA), responsivity (~2.2 × 10^{-3} A/W), and detectivity (~1.6 × 10^{9} Jones), together with the shortest fall time. The enhanced photoresponse is attributed to the improved crystallinity and reduced defect density of the β-Ga_2O_3 nanorods, which facilitate photogenerated carrier transport and suppress carrier recombination. These results demonstrate that optimizing the hydrothermal duration is critical for achieving high-performance Ga_2O_3-based UVC optical sensors.

Keywords: *β-Ga_2O_3 nanorods, graphene oxide, hydrothermal method, UVC optical sensors, wide band gap materials.*

Cite: Duong, M. D., Mai, D. M. D., Nguyen, T. L., Hoang-Nguyen, Q.-A., & Do, H. B. (2026). Optimizing β-Ga_2O_3 nanorod morphology by controlling hydrothermal reaction time for uvc photodetection. *Dong Thap University Journal of Science*, *Online First*, 1-13 https://doi.org/10.52714/dthu.ns.3329.2004

TỐI ƯU HÌNH THÁI THANH NANO β-Ga_2O_3 BẰNG CÁCH ĐIỀU KHIỂN THỜI GIAN PHẢN ỨNG THỦY NHIỆT CHO ỨNG DỤNG PHÁT HIỆN UVC

Dương Minh Đạt[1], Mai Đình Mỹ Duyên[1], Nguyễn Tiến Luật[2], Hoàng Nguyễn Quỳnh Anh[1] và Đỗ Huy Bình[1]*

[1]Khoa Khoa học ứng dụng,
Trường Đại học Công nghệ Kỹ thuật Thành phố Hồ Chí Minh, Việt Nam

[2]Khoa Khoa học và Công nghệ Vật liệu,
Trường Đại học Khoa học Tự nhiên Thành phố Hồ Chí Minh, Việt Nam

**Tác giả liên hệ, Email: binhdh@hcmute.edu.vn*

Lịch sử bài báo

Ngày nhận: 10/4/2026; Ngày nhận chỉnh sửa: 04/6/2026; Ngày duyệt đăng: 11/6/2026

Tóm tắt

Các thanh nano β-Ga_2O_3 được tổng hợp bằng phương pháp thủy nhiệt với thời gian phản ứng 5, 7,5 và 10 giờ nhằm khảo sát ảnh hưởng của thời gian phản ứng đến đặc tính cấu trúc, hình thái và khả năng cảm biến quang UVC. Kết quả nhiễu xạ tia X cho thấy tất cả các mẫu đều hình thành pha β-Ga_2O_3 đơn tà. Khi thời gian thủy nhiệt tăng từ 5 lên 7,5 giờ, chất lượng tinh thể được cải thiện rõ rệt, thể hiện qua sự gia tăng kích thước tinh thể từ 18,3 lên 20,6 nm, đồng thời vi biến dạng mạng và mật độ lệch mạng giảm. Ảnh FE-SEM cho thấy các thanh nano phát triển tương đối đồng đều ở mẫu 7,5 giờ, trong khi thời gian phản ứng kéo dài đến 10 giờ dẫn đến hiện tượng kết tụ và phát triển thứ cấp. Cảm biến quang UVC chế tạo từ mẫu 7,5 giờ cho hiệu năng tốt nhất với dòng quang đạt khoảng 49 nA, độ đáp ứng ~2,2 × 10^{-3} A/W, độ nhạy phát hiện khoảng 1,6 × 10^{9} Jones và thời gian phục hồi ngắn nhất. Hiệu năng quang điện được cải thiện nhờ độ kết tinh cao hơn và mật độ khuyết tật thấp hơn của các thanh nano β-Ga_2O_3, góp phần tăng cường quá trình vận chuyển hạt tải quang sinh và hạn chế sự tái hợp điện tử - lỗ trống. Kết quả nghiên cứu cho thấy việc tối ưu thời gian thủy nhiệt là yếu tố quan trọng để nâng cao hiệu năng của cảm biến quang UVC dựa trên nền vật liệu Ga_2O_3.

Từ khóa: *Cảm biến UVC, graphene oxide, phương pháp thủy nhiệt, thanh nano β-Ga_2O_3, vật liệu vùng cấm rộng.*

1. Introduction

β-Ga_2O_3 has attracted attention for applications in power electronics due to its high critical electric field (~8 MV/cm), and applications in UV optical sensors, photocatalysis, solar cells, and gas sensing for its ultrawide band gap (~4.8 eV) (Do et al., 2022; Pearton et al., 2018). β-Ga_2O_3 can be grown using relatively low-cost crystal growth techniques, including the Czochralski (CZ), floating zone (FZ), and edge-defined film-fed growth (EFG) methods, providing a significant cost advantage over other ultrawide-band-gap semiconductors such as SiC and GaN (Galazka et al., 2017; Kuramata et al., 2016). These characteristics make β-Ga_2O_3 a promising material for solar-blind UVC optical sensors, particularly in secure non-line-of-sight (NLOS) communication systems (Chen et al., 2019). Various low-dimensional β-Ga_2O_3 nanostructures, including nanowires and nanosheets, have been synthesized using wet-chemical methods such as sol-gel, electrospinning, hydrolysis, and hydrothermal growth (Feng et al., 2014; Hailin & Yan, 2013; Hwang et al., 2014; Khan et al., 2006; Kokubun et al., 2007; Kwon et al., 2017; Oh et al., 2016; Reddy et al., 2015; Sharma & Sunkara, 2002; Yoon et al., 2018). Among these methods, hydrothermal synthesis is particularly attractive for its simplicity, low cost, and ability to produce highly crystalline nanostructures (Kang et al., 2014; Wang et al., 2022). Additionally, the morphology of hydrothermally grown β-Ga_2O_3 nanostructures can strongly influence their optical and electrical properties due to changes in aspect ratio, surface states, and charge-carrier dynamics (Reddy et al., 2015; Ryou et al., 2020; Shi & Qiao, 2020). Although templates and surfactants have been used to control nanorod growth, the use of these foreign species may introduce impurities and increase fabrication costs (Pilliadugula & Krishnan, 2018; Zhao et al., 2011).

Despite the large number of studies on β- Ga_2O_3 nanostructures, the applications of Ga_2O_3 nanorods have been limited to pH sensing, glucose sensing (Chou et al., 2023), and the photocatalytic degradation of methylene blue under UVC irradiation (Ryou et al., 2020). Recently, hydrothermally synthesized Ga_2O_3 nanorods have been utilized for UVC optical sensors. However, the reported devices exhibited low performance, with a responsivity of 8.0×10^{-4} A/W and a detectivity of 4.58×10^{9} Jones under 254 nm irradiation (Mao et al., 2025). The limited photoresponse is due to the low electrical conductivity of Ga_2O_3, which restricts charge transport and carrier collection. Nanorod dimensions can also influence oxygen adsorption and desorption, surface trap states, and carrier recombination. However, the role of its morphology, particularly aspect ratio, in UVC photodetection remains poorly understood (Alhalaili et al., 2020). In this study, UVC optical sensors based on hydrothermally synthesized β-Ga_2O_3 nanorods were developed. The effect of hydrothermal duration (5-10 h) on nanorod growth and device performance was systematically examined. To improve charge transport, the synthesized β-Ga_2O_3 nanorods were dispersed in graphene oxide (GO) to create β-Ga_2O_3/GO composite. Since β-Ga_2O_3 exhibits limited electrical conductivity, GO was employed to provide conductive pathways for photogenerated carriers, thereby facilitating charge transport, improving carrier collection efficiency, and enhancing the UVC photoresponse.

2. Materials and Methods

For the synthesis of β-Ga_2O_3 nanorods, 409 mg of $Ga(NO_3)_3$ powder (Sigma-Aldrich) was dissolved in deionized (DI) water to prepare a 0.1 M precursor solution. Subsequently, 16 mL of the solution was transferred into a beaker and stirred at 500 rpm while maintaining the temperature at 80 ^oC. Then, 0.4 mL of 25% NH_4OH solution (Xilong, China) was slowly added. The obtained mixture was transferred into a 25 mL Teflon-lined autoclave and hydrothermally treated at 160 ^oC for 5, 7.5, and 10 h. The resulting samples are denoted as 5

h, 7.5 h, and 10 h samples, respectively. After naturally cooling to room temperature, the precipitates were collected, repeatedly washed with DI water, and dried at 100 °C. Finally, the dried powders were annealed at 910 °C for 3 h with a heating rate of 8 °C/min in air (TCH-M1100-S, Zhengzhou TCH Instrument Co., Ltd) to convert α-GaOOH into β-Ga_2O_3. The final yield of β-Ga_2O_3 powder was ~130 mg. Since β-Ga_2O_3 nanorods are usually dispersed rather than forming a continuous network, an additional pathway is required to support carrier transport. Therefore, graphene oxide was used as a conductive medium because of its ability to interconnect isolated nanostructures.

The preparation process of GO was described in our previous work (Do et al., 2024). β-Ga_2O_3/GO composite films were fabricated via a vacuum filtration process. To prepare the β-Ga_2O_3/GO suspension, β-Ga_2O_3 nanorod powder was mixed with GO powder in deionized water, maintaining a mass ratio of 3:1 (GO:β-Ga_2O_3). Since this study mainly focuses on the effect of hydrothermal time on the properties of Ga_2O_3 nanorods, the GO:Ga_2O_3 ratio was kept constant throughout the experiments, although this ratio can influence the photoresponse behavior and dark current of the device. The effect of the GO:Ga_2O_3 ratio requires further investigation and will be presented in a separate study. The β-Ga_2O_3/GO concentration was kept to 3 mg/mL, and the mixture was sonicated for more than 1 h to ensure complete dispersion. After that, 3 mL of the suspension was filtered through a membrane with a pore size of 0.22 µm, forming a thin β-Ga_2O_3/GO layer on the filter surface. The film was left to dry naturally at room temperature shown in Fig. 1(a) with the thickness of ~18.7 um shown in Fig. 1(b). Ti/W electrodes (5 pairs) with the length of 1.8 mm and the channel distance of 50 µm were deposited onto the β-Ga_2O_3/GO film using a shadow mask shown in Fig. 1(c), via DC magnetron sputtering. The devices were heated in air at 130 °C for 1 min to reduce resistance between the Ti/W electrodes and the β-Ga_2O_3/GO film. The final device structure is presented in Fig. 1(d).

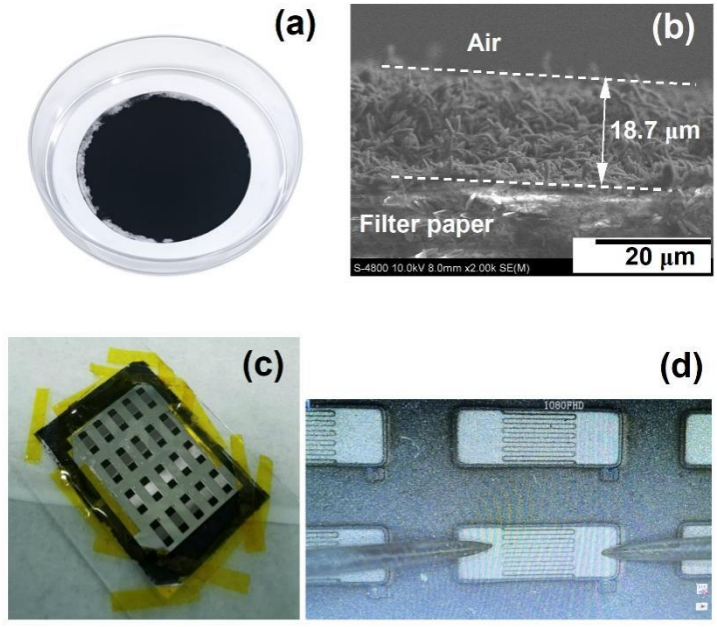

Figure 1. Photographs of the β-Ga_2O_3/GO film and the fabricated device. (a) As-prepared β-Ga_2O_3/GO film. (b) Cross-sectional SEM image of the deposited β-Ga_2O_3/GO on filter paper, showing a thickness of ~18.7 µm. (c) Device structure with patterned electrodes defined by a shadow mask. (d) Optical microscope image showing the electrode configuration used for electrical measurements.

The morphology of the β-Ga_2O_3 nanorods was checked using a field-emission scanning electron microscope (FESEM, S-4800, Hitachi, Japan). Crystalline characteristics were inspected by X-ray diffraction (XRD) using a multipurpose Empyrean diffractometer (Malvern Panalytical, UK). The chemical bonding in the β-Ga_2O_3 nanorods was determined using Fourier-transform infrared (FTIR) spectroscopy (Nicolet 6700, Thermo Scientific, USA). For device characterization, the photocurrent and responsivity of the β-Ga_2O_3/GO UVC optical sensors were measured at a bias of 10 V under 254 nm illumination, with a power density of 2.6 mW/cm² . The distance between the light source and the β-Ga_2O_3/GO device was fixed at 4.7 cm, and the light intensity was measured using a Lutron UVC-254A UV Light Meter. All electrical measurements were conducted using an Ossila P2005A2 source measurement unit (SMU, Ossila, UK).

3. Results and Discussion

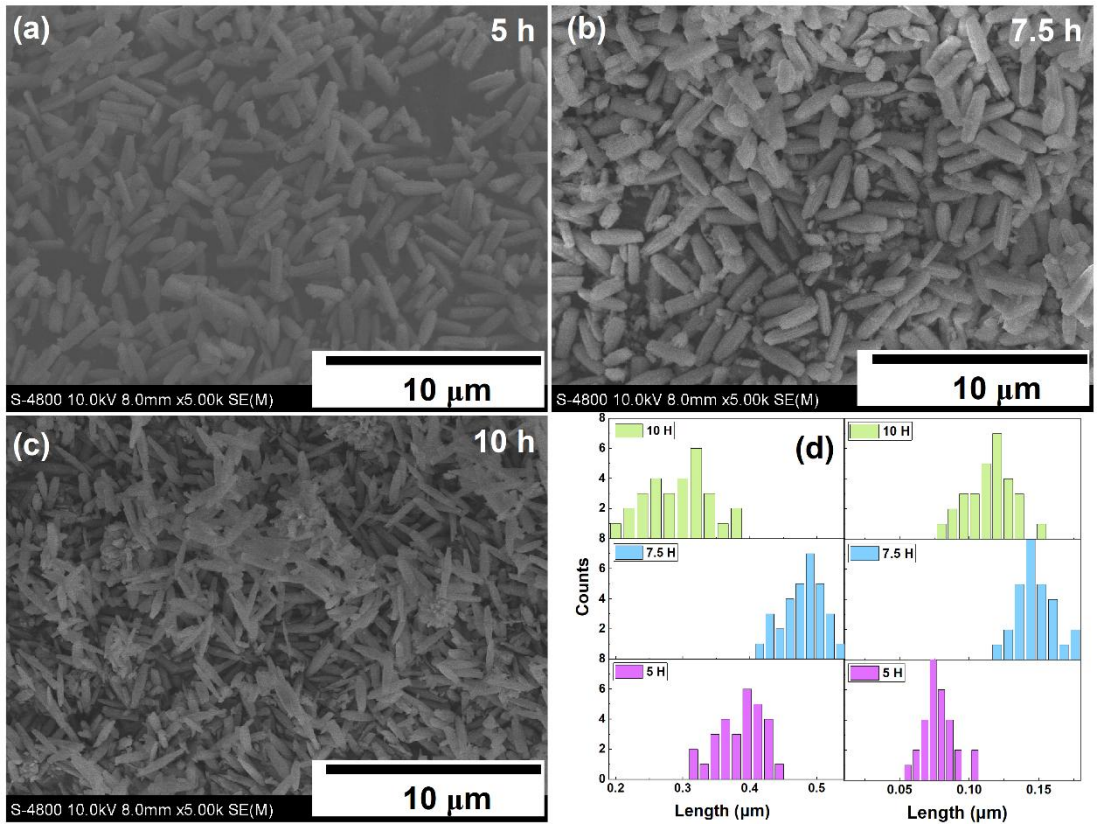

Figure 2. FE-SEM images of β-Ga_2O_3 nanorods obtained at different hydrothermal durations: (a) 5 h, (b) 7.5 h, and (c) 10 h, along with (d) the corresponding statistical distributions of nanorod length and width.

Figure 2 shows the evolution of β-Ga_2O_3 nanostructures with hydrothermal time. Compared with the 5 h sample (Fig. 2(a)), the 7.5 h sample (Fig. 2(b)) exhibits well-defined nanorods with a more uniform size distribution. In the 10 h sample (Fig. 2(c)), noticeable aggregation and overlapping of the nanorods are observed, resulting in a less uniform morphology. The aspect ratio (length/width) of the β-Ga_2O_3 nanorods, extracted from the histogram shown in Fig. 2(d), changed slightly with hydrothermal duration, varying from 3.39 ± 0.61 for the 5 h sample to 3.26 ± 0.41 for the 7.5 h sample and 3.72 ± 0.79 for the 10 h sample. These results suggest that the overall rod-like morphology was maintained throughout the hydrothermal growth process. Notably, the 7.5 h sample exhibited the

narrowest aspect-ratio distribution, indicating improved morphological uniformity. In contrast, the 10 h sample showed both a higher average aspect ratio and a broader distribution, suggesting enhanced longitudinal growth accompanied by increased size dispersion.

X-ray diffraction patterns (Fig. 3) confirm that all samples crystallized in the monoclinic β-Ga_2O_3 phase, with diffraction peaks matching well with the standard PDF 76-0573 data. β-Ga_2O_3 possesses a monoclinic crystal structure with lattice parameters of a = 12.23 Å, b = 3.04 Å, c = 5.80 Å, and angles α = 90°, β = 103.7°, and γ = 90° (Mi et al., 2012). After calcination at 910 °C for 3 h, no secondary phases were detected in any sample. Although the diffraction peak positions remained unchanged with hydrothermal time, noticeable differences in peak broadening were observed. Compared with the 5 h sample, the 7.5 h sample exhibited sharper diffraction peaks, indicating improved crystallinity. Further increasing the hydrothermal duration to 10 h resulted in minor changes in the diffraction profiles, suggesting that the crystal quality approached a stable state after 7.5 h.

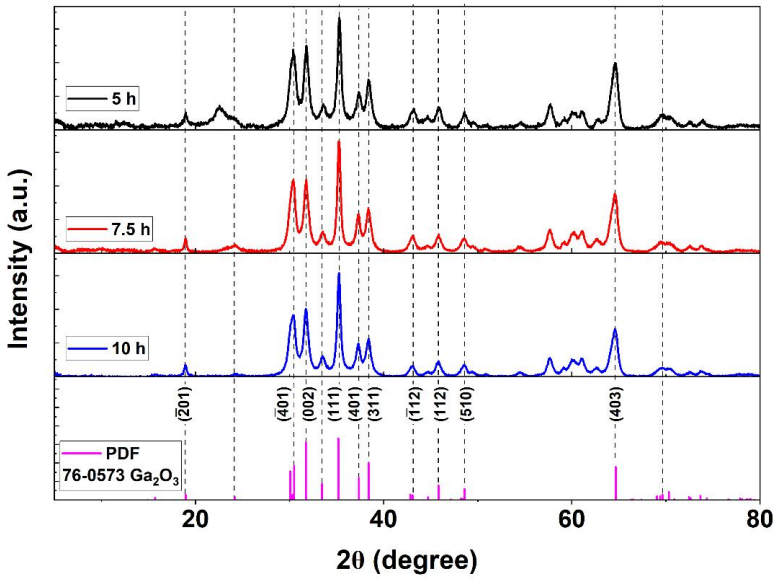

Figure 3. XRD patterns of β-Ga_2O_3 nanorods synthesized via hydrothermal method at different reaction times (5, 7.5, and 10 h) and calcinated at 910 °C for 3 h.

The FTIR spectra shown in Fig. 4 provide information about the bonding in the obtained samples. A broad peak in the region around ~3400 cm^{-1}, together with a weaker band near ~1630 cm^{-1}, is related to O–H vibrations (Li et al., 2010). A band observed near ~1380 cm^{-1} can be associated with Ga–OH species (Li et al., 2010). Although the sample was annealed at 910 °C, the absorption band related to –OH species can still be observed in the FTIR spectrum. This behavior is likely associated with surface hydroxyl groups or water molecules adsorbed on the β-Ga_2O_3 surface after exposure to air, rather than the presence of residual GaOOH phase. At lower wavenumbers, the spectra show distinct absorptions around ~670 cm^{-1} and ~450 cm^{-1} (Yang et al., 2009). These features correspond to Ga–O–Ga and Ga–O vibrations, respectively, confirming the presence of the gallium oxide framework and the formation of β-Ga_2O_3.

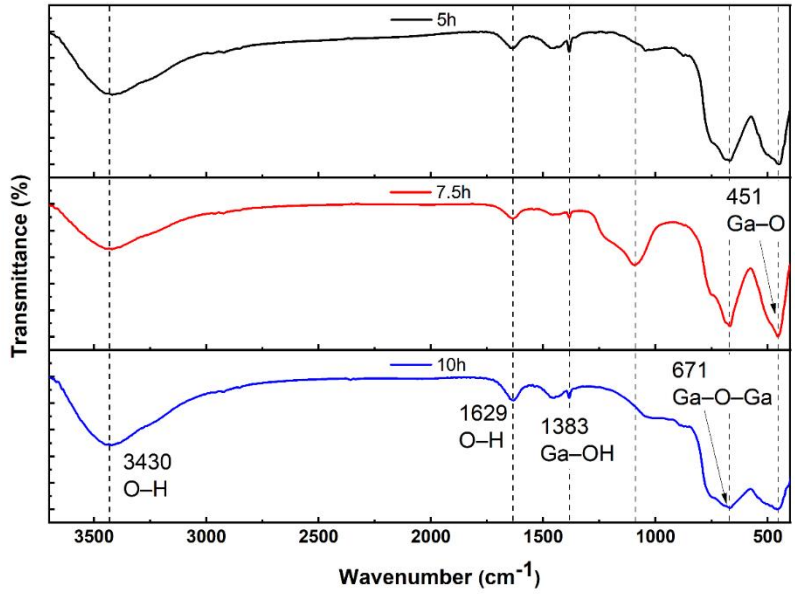

Figure 4. FTIR spectra of β-Ga_2O_3 nanorods synthesized at different hydrothermal durations (5, 7.5, and 10 h)

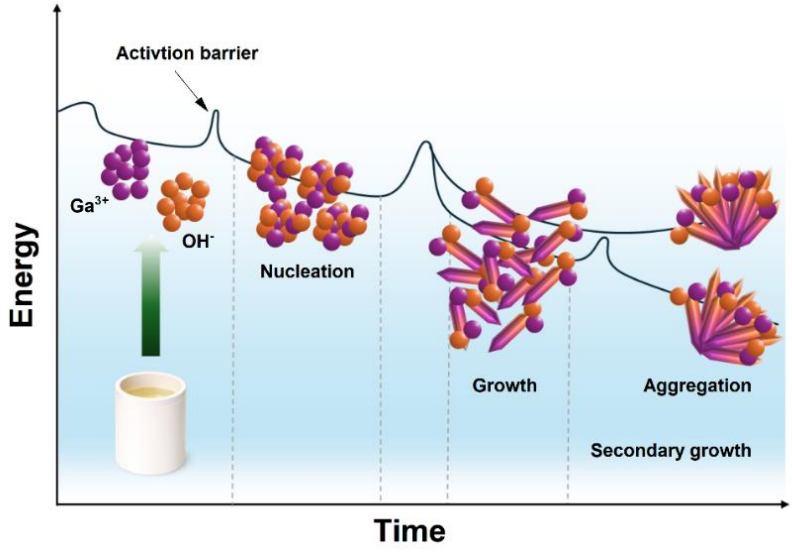

Figure 5. Schematic representation of the formation of α-GaOOH nanorods during the hydrothermal process.

To clarify the possible growth mechanism of the GaOOH nanorods, Fig. 5 schematically illustrates the morphological evolution during the hydrothermal process. Under alkaline conditions, Ga^{3+} ions are expected to react with OH^- ions to form gallium hydroxide species, which subsequently dehydrate into GaOOH nuclei (Qian et al., 2008). The high concentration of OH^- ions and the alkaline environment may facilitate anisotropic growth by preferentially adsorbing on specific crystal facets. During the early growth stage, small GaOOH nanoparticles are formed and gradually grow into rod-like structures through dissolution and recrystallization (Guo et al., 2013; Lee et al., 2005). This evolution is consistent with the relatively separated nanorods observed in the 5 h sample (Fig. 2(a)). With

increasing hydrothermal duration, the nanorods become more distinct and densely distributed, as observed for the 7.5 h sample (Fig. 2(b)), suggesting improved crystal growth and structural organization. However, prolonged reaction time may promote nanorod aggregation, leading to the clustered structures observed in the 10 h sample (Fig. 2(c)).

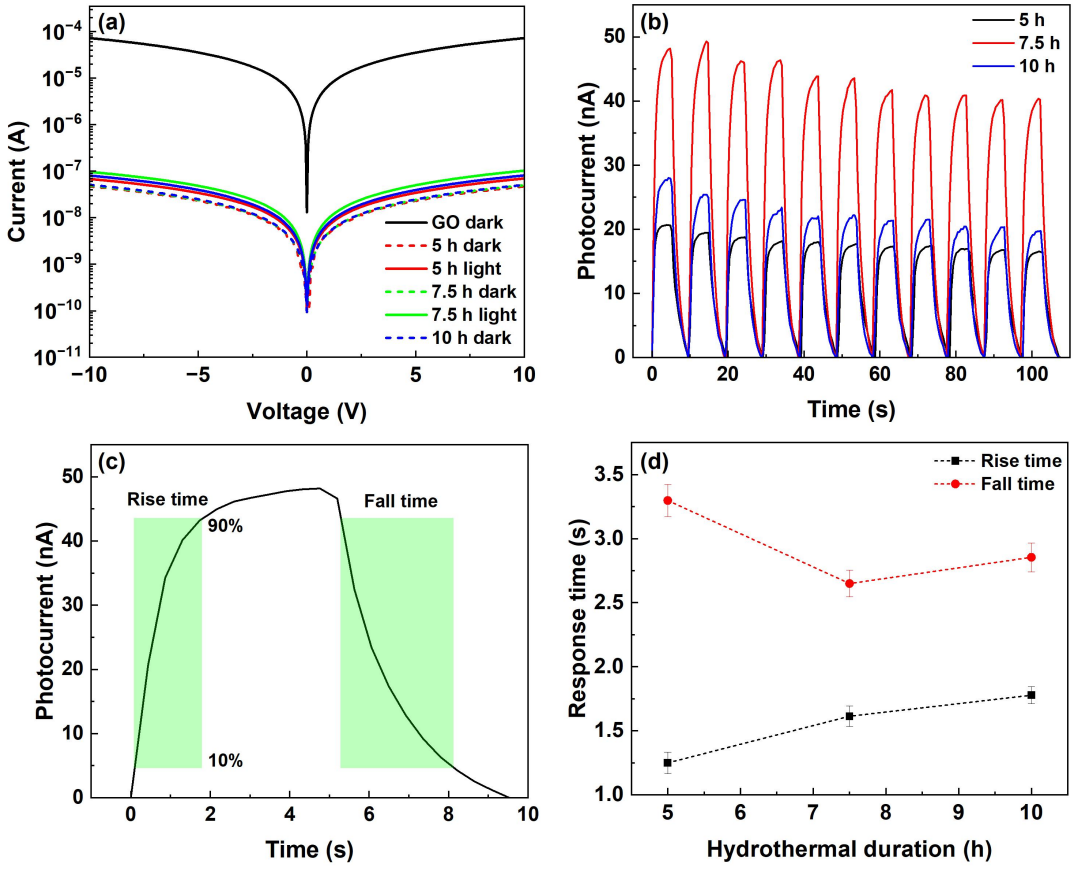

Figure 6. (a) I-V characteristics of the GO-based UVC optical sensors hydrothermally treated for 5, 7.5, and 10 h under dark and UV illumination conditions. The pristine GO sample exhibits significantly higher dark current compared to β-Ga_2O_3/GO samples. (b) I-t curves of the devices under periodic UV light switching. (c) Schematic illustration of the rise time and fall time determination. (d) Variation of rise and fall times as a function of hydrothermal duration.

Figure 6(a) presents the I-V curves of pristine GO and β-Ga_2O_3/GO devices under dark conditions and 254 nm illumination (2.6 mW/cm²). The pristine GO device exhibits a high dark current, yielding little difference between the dark and illuminated currents. In contrast, the β-Ga_2O_3/GO devices show a dark current reduction of about 3 orders of magnitude and a clear current difference under illumination, particularly for the 7.5 h sample. Figure 6(b) presents the current-time (*I-t*) curves of the devices under periodic UVC illumination. The photocurrent (I_{ph}) is obtained by subtracting the dark current (I_{dark}) from the light current (I_{light}) (Do et al., 2026):

$$I_{ph} = I_{light} - I_{dark}. \quad (1)$$

All devices illustrated stable and repeatable photoresponse characteristics. The 7.5 h sample had the highest photocurrent (~49 nA), whereas a decrease was observed for the 10 h sample, due to the increase in carrier recombination and structural agglomeration shown in Fig. 2(c).

Incomplete recovery of surface oxygen species during repeated illumination cycles may contribute to the gradual photocurrent decay shown in Fig. 6(b). Figure 6(c) shows the determination of the rise time (τ_{rise}) and the fall time (τ_{fall}), specified by the period required for I_{ph} to increase from 10% to 90% and decrease from 90% to 10% of its maximum value, respectively. Compared with the 5 h sample, the 7.5 h sample showed both a longer τ_{rise} (1.61 s), and a higher I_{ph}, implying more efficient photocarrier generation and transport in this sample. In contrast, the 10 h sample revealed a lower I_{ph} (Fig. 6(b)) and a longer τ_{rise} (Fig. 6(d)), indicating less efficient photocarrier transport in this sample. Among all samples, the 7.5 h sample exhibited the shortest τ_{fall} of 2.74 s.

The responsivity (R) and detectivity (D^*) are determined from (Singh et al., 2024):

$$R = \frac{J_{ph}}{P}, \tag{2}$$

$$D^* = \frac{R\sqrt{A}}{\sqrt{2qI_{dark}}}, \tag{3}$$

where J_{ph} is the photocurrent density, P is the incident light power density, A is the effective device area, I_{dark} is the dark current, and q is the elementary charge. Fig. 7(a) shows that both responsivity and detectivity are strongly influenced by the hydrothermal duration. The 7.5 h sample exhibits the best photoresponse performance, with the R reaching $(2.24 \pm 0.06) \times 10^{-3}$ A/W and the D* achieving $(1.61 \pm 0.04) \times 10^{9}$ Jones. Notably, the responsivity obtained in this work is approximately 2.5 times higher than that reported in the most recent related study (Mao et al., 2025). This improvement can be correlated with the enhanced crystallinity derived in Fig. 7(b), where the crystallite size is calculated from Fig. 3 using Scherrer's equation (Şenaslan et al., 2021)):

$$D = \frac{0.9\lambda}{\beta cos\theta}, \tag{4}$$

where λ denotes the X-ray wavelength, β is the full width at half maximum (FWHM) of the diffraction peak expressed in radians, and θ represents the Bragg angle. Figure 7(b) indicates that the crystallite size increased from 18.3 nm for the 5 h sample to 20.5 nm for the 7.5 h sample, followed by a slight decrease to 19.8 nm for the 10 h sample. Meanwhile, the aspect ratio (calcultated from Fig. 2(d)) decreased slightly from 3.39 ± 0.61 to 3.26 ± 0.41 and then increased to 3.72 ± 0.79 with further increasing hydrothermal duration. The lowest aspect ratio observed for the 7.5 h sample, together with its largest crystallite size, suggests improved crystal growth while maintaining a relatively uniform nanorod morphology. The dislocation density (δ) and microstrain (ε) were calculated using Eqs. (5) and (6), respectively (Şenaslan et al., 2021):

$$\delta = \frac{1}{D^2}, \tag{5}$$

$$\varepsilon = \frac{\beta}{4tan\theta}. \tag{6}$$

Figure 7(c) indicates that the dislocation density and microstrain decreased from the 5 h sample to the 7.5 h sample and then slightly increased for the 10 h sample. The lowest values obtained for the 7.5 h sample indicate reduced lattice defects and crystal distortion, resulting in improved crystallinity shown in Fig. 7(b). These factors reduce carrier recombination and improve the UVC photoresponse. The higher photocurrent of the 7.5 h sample originates from improved crystallinity, reduced defect density, and a more homogeneous nanorod morphology. The proposed photoresponse mechanism of the β-Ga_2O_3/GO devices under UVC irradiation is illustrated in Fig. 7(d). In ambient air, various gas species may adsorb

onto the β-Ga_2O_3 surface, and oxygen molecules are considered the primary active species because of their strong electron-withdrawing capability (Khanh et al., 2026). In dark, these adsorbed oxygen molecules trap electrons from the β-Ga_2O_3 nanorods and form surface oxygen ions (O^{2-}), reducing the free carrier concentration and resulting in a relatively low dark current. In UVC illumination, electron-hole pairs are generated in the β-Ga_2O_3 nanorods. The photogenerated electrons are transported to the GO layer through the heterointerface, while the holes move toward the β-Ga_2O_3 surface. So, the holes recombine with the adsorbed oxygen ions, causing the desorption of oxygen molecules from the surface. This process decreases the depletion effect at the surface and increases the carrier concentration, leading to an increase in photocurrent under UVC irradiation.

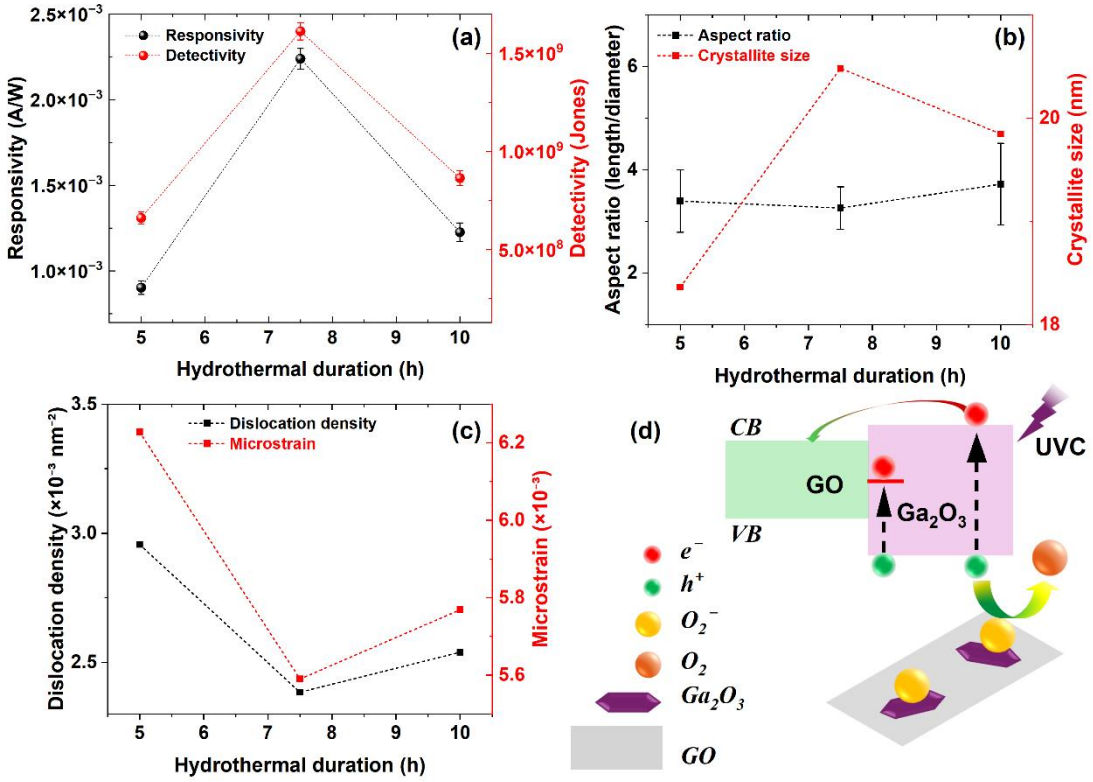

Figure 7. Correlation between structural properties and UVC photodetection performance of β-Ga_2O_3/GO devices: (a) responsivity and detectivity, (b) aspect ratio and crystallite size, (c) dislocation density and microstrain, and (d) proposed photoresponse mechanism.

4. Conclusion

In summary, β-Ga_2O_3 nanorods prepared at different hydrothermal durations illustrated distinct morphological and structural characteristics. The 7.5 h sample showed the balance between nanorod uniformity, aspect ratio, and crystal quality. Structural characterization confirmed the transformation of the α-GaOOH into monoclinic β-Ga_2O_3 after annealing at 910°C. All fabricated β-Ga_2O_3/GO UVC optical sensors exhibited stable and repeatable photoresponse characteristics. The device based on the 7.5 h sample delivered the best performance, with a responsivity of 2.24 × 10^{-3} A/W, a rise time of ~1.61 s, and a fall time of ~2.74 s at 10 V. Its responsivity is approximately 2.5 times higher than that reported in the most recent related study. These findings indicate that optimizing the

hydrothermal duration is essential for achieving high-performance β-Ga_2O_3-based UVC optical sensors.

Acknowledgements: This work received funding under project grant No: B2024-SPK-05 from the Ministry of Education and Training and was hosted by Ho Chi Minh City University of Technology and Engineering, Vietnam.

References

Alhalaili, B., Bunk, R. J., Mao, H., Cansizoglu, H., Vidu, R., Woodall, J., & Islam, M. S. (2020). Gallium oxide nanowires for UV detection with enhanced growth and material properties. *Scientific Reports*, *10*(1), 21434. https://doi.org/10.1038/s41598-020-78326-x

Chen, X., Ren, F., Gu, S., & Ye, J. (2019). Review of gallium-oxide-based solar-blind ultraviolet photodetectors. *Photonics Research*, *7*(4), 381-415. https://doi.org/10.1364/prj.7.000381

Chou, H.-Y., Yadlapalli, B. K., Yen, C.-C., Singh, A. K., Chiang, J.-L., & Wuu, D.-S. (2023). Ga2O3 nanorods synthesized by hydrothermal method for dual-functional sensing of pH value and glucose. *Sensors and Actuators A: Physical*, *363*, 114695. https://doi.org/https://doi.org/10.1016/j.sna.2023.114695

Do, H.-B., Le, D.-N., Nguyen, T.-H., Nguyen, V. T., Phan-Gia, A.-V., Hien, T. D., Le, H.-M., Pham, P. V., De Souza, M. M., & Nguyen Dang, N. (2024). Recycling of reduced graphene oxide from graphite rods in disposable zinc battery applicable to optical sensing. *Ceramics International*, *50*(21, Part C), 43754-43762. https://doi.org/https://doi.org/10.1016/j.ceramint.2024.08.228

Do, H.-B., Nguyen, T.-H., Ngo, T.-H.-L., Phan-Gia, A.-V., Nguyen-Thuy-Ngoc, T., Huynh, T.-L., & Nguyen-Dang, N. (2026). Ga2O3-graphene oxide hybrid optical sensor. *Materials Letters*, *404*, 139602. https://doi.org/https://doi.org/10.1016/j.matlet.2025.139602

Do, H.-B., Phan-Gia, A.-V., Nguyen, V. Q., & De Souza, M. M. (2022). Optimization of normally-off β-Ga2O3 MOSFET with high Ion and BFOM: A TCAD study. *AIP Advances*, *12*(6). https://doi.org/10.1063/5.0094418

Feng, W., Wang, X., Zhang, J., Wang, L., Zheng, W., Hu, P., Cao, W., & Yang, B. (2014). Synthesis of two-dimensional β-Ga_2O_3 nanosheets for high-performance solar blind photodetectors. *Journal of Materials Chemistry C 2*(17), 3254-3259.

Galazka, Z., Uecker, R., Klimm, D., Irmscher, K., Naumann, M., Pietsch, M., Kwasniewski, A., Bertram, R., Ganschow, S., & Bickermann, M. (2017). Scaling-Up of Bulk β-Ga2O3 Single Crystals by the Czochralski Method. *ECS Journal of Solid State Science and Technology*, *6*(2), Q3007. https://doi.org/10.1149/2.0021702jss

Guo, D., Xie, G., & Luo, J. (2013). Mechanical properties of nanoparticles: basics and applications. *Journal of Physics D: Applied Physics*, *47*(1), 013001.

Hailin, M., & Yan, L. (2013). One-Step Preparation of β-Ga2O3 Nanomaterial and Research the Electrical Transport Properties at High Temperature. *Rare Metal Materials and Engineering*, *42*(11), 2245-2247.

Hwang, W. S., Verma, A., Peelaers, H., Protasenko, V., Rouvimov, S., Seabaugh, A., Haensch, W., de Walle, C. V., Galazka, Z., & Albrecht, M. (2014). High-voltage

field effect transistors with wide-bandgap β-Ga_2O_3 nanomembranes. *Applied Physics Letters*, *104*(20).

Kang, B., Mang, S., Song, K., Lee, K., & Yoon, D. (2014). Hydrothermal synthesis and characterization of uniform β-Ga_2O_3 hollow nanostructures by carbon nanospheres. *J. Ceram. Process. Res*, *15*(3), 200-203.

Khan, A., Jadwisienczak, W. M., & Kordesch, M. E. (2006). One-step preparation of ultra-wide β-Ga2O3 microbelts and their photoluminescence study. *Physica E: Low-dimensional Systems and Nanostructures*, *35*(1), 207-211.

Khanh, N., Do, H.-B., Nguyen, T.-H., Ngo, T.-H.-L., Phan-Gia, A.-V., Tran, T. T. V., De Souza, M. M., Le, H.-M., Linh, L., Nawaz, M. H., Chuang, F.-C., Pham, P. V., & Nguyen Dang, N. (2026). Defect-Controlled Photoresponse in GaOOH/Reduced Graphene Oxide Composites for Ultraviolet-C Photodetectors. *ACS Applied Electronic Materials*, *8*(9), 4336-4342. https://doi.org/10.1021/acsaelm.6c00519

Kokubun, Y., Miura, K., Endo, F., & Nakagomi, S. (2007). Sol-gel prepared β-Ga_2O_3 thin films for ultraviolet photodetectors. *Applied Physics Letters*, *90*(3).

Kuramata, A., Koshi, K., Watanabe, S., Yamaoka, Y., Masui, T., & Yamakoshi, S. (2016). High-quality β-Ga_2O_3 single crystals grown by edge-defined film-fed growth. *Japanese Journal of Applied Physics*, *55*(12), 1202A1202. https://doi.org/10.7567/jjap.55.1202a2

Kwon, Y., Lee, G., Oh, S., Kim, J., Pearton, S. J., & Ren, F. (2017). Tuning the thickness of exfoliated quasi-two-dimensional β-Ga_2O_3 flakes by plasma etching. *Applied Physics Letters*, *110*(13).

Lee, E. J., Ribeiro, C., Longo, E., & Leite, E. R. (2005). Oriented attachment: An effective mechanism in the formation of anisotropic nanocrystals. *The Journal of Physical Chemistry B*, *109*(44), 20842-20846.

Li, G., Peng, C., Li, C., Yang, P., Hou, Z., Fan, Y., Cheng, Z., & Lin, J. (2010). Shape-controllable synthesis and morphology-dependent luminescence properties of GaOOH: Dy^{3+} and β-Ga_2O_3: Dy^{3+}. *Inorganic Chemistry*, *49*(4), 1449-1457.

Mao, L., Wang, X., Huang, C., Ma, Y., Qin, F., Lu, W., Zhu, G., Shi, Z., Cui, Q., & Xu, C. (2025). Controllable hydrothermal synthesis of 1D β-Ga_2O_3 for solar-blind ultraviolet photodetection. *Nanomaterials*, *15*(5), 402. https://www.mdpi.com/2079-4991/15/5/402

Mi, W., Ma, J., Luan, C., Lv, Y., Xiao, H., & Li, Z. (2012). Characterization of β-Ga_2O_3 epitaxial films grown on MgO (111) substrates by metal-organic chemical vapor deposition. *Materials Letters*, *87*, 109-112. https://doi.org/https://doi.org/10.1016/j.matlet.2012.07.106

Oh, S., Kim, J., Ren, F., Pearton, S. J., & Kim, J. (2016). Quasi-two-dimensional β-gallium oxide solar-blind photodetectors with ultrahigh responsivity. *Journal of Materials Chemistry C 4*(39), 9245-9250.

Pearton, S. J., Yang, J., Cary, P. H., IV, Ren, F., Kim, J., Tadjer, M. J., & Mastro, M. A. (2018). A review of Ga_2O_3 materials, processing, and devices. *Applied Physics Reviews*, *5*(1). https://doi.org/10.1063/1.5006941

Pilliadugula, R., & Krishnan, N. G. (2018). Gas sensing performance of GaOOH and β-Ga_2O_3 synthesized by hydrothermal method: a comparison. *Materials Research Express*, *6*(2), 025027.

Qian, H.-S., Gunawan, P., Zhang, Y.-X., Lin, G.-F., Zheng, J.-W., & Xu, R. (2008). Template-free synthesis of highly uniform α-GaOOH spindles and conversion to α-Ga_2O_3 and β-Ga_2O_3. *Crystal Growth and Design*, *8*(4), 1282-1287.

Reddy, L. S., Ko, Y. H., & Yu, J. S. (2015). Hydrothermal synthesis and photocatalytic property of β-Ga_2O_3 nanorods. *Nanoscale Research Letters*, *10*, 1-7.

Ryou, H., Yoo, T. H., Yoon, Y., Lee, I. G., Shin, M., Cho, J., Cho, B. J., & Hwang, W. S. (2020). Hydrothermal synthesis and photocatalytic property of Sn-doped β-Ga_2O_3 nanostructure. *ECS Journal of Solid State Science and Technology*, *9*(4), 045009. https://doi.org/10.1149/2162-8777/ab8b4b

Şenaslan, F., Taşdemir, M., & Çelik, A. (2021). Effect of working pressure and post-annealing on structural, optical and electrical properties of p-type NiO thin films produced by RF magnetron sputtering technique. *Applied Physics A*, *127*(10), 739. https://doi.org/10.1007/s00339-021-04901-2

Sharma, S., & Sunkara, M. K. (2002). Direct synthesis of gallium oxide tubes, nanowires, and nanopaintbrushes. *Journal of the American Chemical Society*, *124*(41), 12288-12293.

Shi, F., & Qiao, H. (2020). Influence of hydrothermal reaction time on crystal qualities and photoluminescence properties of β-Ga_2O_3 nanorods. *Journal of Materials Science: Materials in Electronics*, *31*, 20223-20231.

Singh, N. S., Mia, A. K., & Giri, P. (2024). Role of oxygen functional groups and attachment of Au nanoparticles on graphene oxide sheets for improved photodetection performance. *Nanoscale Advances*, *6*(8), 2136-2148. https://doi.org/10.1039/D3NA01120H

Wang, X., Qiao, H., Liu, T., Song, F., An, Z., Xu, Y., Zhang, L., & Shi, F. (2022). Ultraviolet photoluminescence of β-Ga_2O_3 microparticles synthesized by hydrothermal method. *Journal of Materials Science: Materials in Electronics*, *33*(16), 13040-13050.

Yang, J. J., Zhao, Y., & Frost, R. L. (2009). Infrared and infrared emission spectroscopy of gallium oxide α-GaO (OH) nanostructures. *Spectrochimica Acta Part A: Molecular and Biomolecular Spectroscopy*, *74*(2), 398-403.

Yoon, Y., Han, K. I., Kim, B. H., Lee, I. G., Kim, Y., Kim, J. P., & Hwang, W. S. (2018). Formation of β-Ga2O3 nanofibers of sub-50 nm diameter synthesized by electrospinning method. *Thin Solid Films*, *645*, 358-362.

Zhao, W., Yang, Y., Hao, R., Liu, F., Wang, Y., Tan, M., Tang, J., Ren, D., & Zhao, D. (2011). Synthesis of mesoporous β-Ga_2O_3 nanorods using PEG as template: Preparation, characterization and photocatalytic properties. *Journal of Hazardous materials*, *192*(3), 1548-1554.